

## Article

# Identification of Chiral-Specific Carbon Nanotube Binding Peptides Using a Modified Biopanning Method

Rachel Krabacher <sup>1,2,3</sup>, Steve Kim <sup>3</sup> , Yen Ngo <sup>3</sup>, Joseph Slocik <sup>1</sup>, Christina Harsch <sup>1</sup> and Rajesh Naik <sup>3,\*</sup>

<sup>1</sup> Materials & Manufacturing Directorate, Air Force Research Laboratory, Wright-Patterson AFB, Dayton, OH 45433, USA; rachel.krabacher.1@us.af.mil (R.K.); joseph.slocik.ctr@us.af.mil (J.S.); christina.harsch.ctr@us.af.mil (C.H.)

<sup>2</sup> Chemical Engineering, University of Dayton, Dayton, OH 45409, USA

<sup>3</sup> 711th Human Performance Wing, Air Force Research Laboratory, Wright-Patterson AFB, Dayton, OH 45433, USA; steve.kim.13@us.af.mil (S.K.); yenngo43@yahoo.com (Y.N.)

\* Correspondence: rajesh.naik@us.af.mil; Tel.: +1-937-785-8222

**Abstract:** Peptides can recognize and selectively bind to a wide variety of materials dependent on both their surface properties and the environment. Biopanning with phage or cell peptide display libraries can identify material-specific binding peptides. However, the limitations with sequence diversity of traditional bacteriophage (phage) display libraries and loss of unique phage clones during the amplification cycles results in a smaller pool of peptide sequences identified. False positive sequences tend to emerge during the biopanning process due to highly proliferating, yet nonspecific, phages. In order to overcome this limitation of traditional biopanning methodology, a modified method using high-throughput next generation sequencing (HTS) was tested to select for unique peptides specific to two types of single wall carbon nanotube (SWNTs) sources with varying diameter distribution and chirality. Here, the process, analysis, and characterization of peptide sequences identified using the modified method is further described and compared to a peptide identified in literature using the traditional method. Selected sequences from this study were incorporated in a SWNT dispersion experiment to probe their selectivity to the nanotube diameter. We show that NHTS can uncover unique binding sequences that might have otherwise been lost during the traditional biopanning method.

**Keywords:** biorecognition element; carbon nanotube; biopanning; peptide; bacteriophage display; biosensor; high throughput next generation sequencing



**Citation:** Krabacher, R.; Kim, S.; Ngo, Y.; Slocik, J.; Harsch, C.; Naik, R. Identification of Chiral-Specific Carbon Nanotube Binding Peptides Using a Modified Biopanning Method. *Chemosensors* **2021**, *9*, 245. <https://doi.org/10.3390/chemosensors9090245>

Academic Editors: Sherif Moussa, Andrea Ponzoni and Boris Lakard

Received: 10 June 2021

Accepted: 25 August 2021

Published: 1 September 2021

**Publisher's Note:** MDPI stays neutral with regard to jurisdictional claims in published maps and institutional affiliations.



**Copyright:** © 2021 by the authors. Licensee MDPI, Basel, Switzerland. This article is an open access article distributed under the terms and conditions of the Creative Commons Attribution (CC BY) license (<https://creativecommons.org/licenses/by/4.0/>).

## 1. Introduction

Single-walled carbon nanotubes (SWNTs) have extraordinary electronic properties that make them a desirable material to use in various high performance electronic, optical, and optoelectronic sensing platforms. The additional chemical and mechanical stability of SWNTs is promising for molecular level chemical and biochemical sensors by forming a direct interface with chem/bio receptors. Structurally, SWNTs are composed of thin sheets of graphene rolled in specific orientations (lattice angle), dependent on methods of synthesis. The orientation in which the SWNTs are rolled determines the (n, m) chirality, which enables unique physiochemical and electrical diversity including being metallic or semiconducting [1–4]. Due to their nanometer (nm) scale diameter and high aspect ratio, SWNTs offer a high degree of chemical and biochemical functionalization allowing them to provide an optimal platform for sensor applications [5]. Functionalization of SWNTs with biorecognition elements for sensor applications requires the elements to be specific and selective towards the analyte of choice.

Peptides known to bind to materials are used as interfaces to functionalize surfaces for a variety of applications. These include: improved detection of biomarkers to improve cancer diagnosis by way of fluorescently labeled peptides [6], peptide functionalized

gold nanoparticles to act as biorecognition elements in the detection of colorectal carcinomas [7], and peptide functionalized SWNT field effect transistors to monitor volatile organic compounds in breath [8]. Engineering peptides with specific material binding affinities allows for multifunctional properties, for example, carbon nanotube and gold binding peptides can be engineered to have bifunctional properties of both nanomaterial and analyte binding.

Phage display (PD) has been used to select high affinity recognition peptides for specific materials. PD is an established and effective tool that exploits the use of an M13 phage library containing random pentavalent-expressed peptide sequences ( $\sim 10^{12}$ ) to select specific peptides against a target of choice (i.e., SWNTs). In short, the M13 phage library is exposed to a target of interest, where some peptides bind to the target, while other nonbinding peptides remain in solution. This binding is specific to the desired target properties, environment, and peptide sequence interactions. Electrostatic forces, hydrogen bonding, van der Waals forces, and London dispersion forces can all contribute to the specific binding of peptides to a target of choice [9]. Nonbinding phage are removed and discarded, while bound phage are eluted off the target surface, replicated, and kept for sequencing. Multiple rounds of exposure, removal, replication, and sequencing allow for identification of peptides with an affinity to a specific target. Previous work conducted by Pender, et al. used traditional PD methods to identify the P1 peptide (HSSYWYAFNNKT) preferentially binding to carbon nanotubes [10]. While traditional PD methods have allowed for an easy and low cost way of identifying peptide sequences that bind to a target of interest from a very large population, they are prone to the known sequence biases [11–13].

The traditional PD is biased due to the varying rates of phage amplification that tend to cloud enrichment as sequences with high rates of amplification yet low binding affinity outcompete high affinity binding sequences. This bias along with the inherent amino acid bias within the library clouds the results even further. Moreover, Sanger sequencing limits sequencing to a small fraction of the sample. Such a snapshot representative of the library makes it difficult to fully exploit the sample diversity often leading to a loss of potential high affinity highly selective binders.

The development of next generation sequencing platforms has allowed for a high throughput sequencing (HTS) option to be used in conjunction with PD in place of traditional Sanger sequencing [14]. While these methods have allowed for a more complete understanding of peptide enrichment, the data often contains parasitic fast-growing phages that may appear as specific binding sequences. In other words, amplification bias and the large amount of data make it difficult to identify and remove low affinity fast-growing sequences in order to uncover true high affinity binding peptides.

Here, we report PD combined with three different analysis methods to determine the most effective method of identifying highly specific SWNT binders. PD combined with Sanger sequencing (referenced throughout as traditional sequencing) and PD combined with traditional HTS (HTS–PD) were compared to a unique normalized HTS analysis method (NHTS–PD). This method, unlike traditional and HTS–PD methods, combines experimental PD (with and sans SWNT targets) with analytical programming to (1) identify persistent parasitic sequences throughout the panning process and (2) uncover unique material-specific binding peptides. Sequences from all three methods were characterized and compared for high affinity and specificity.

## 2. Materials and Methods

HiPCO<sup>TM</sup> and CoMoCAT (SG65<sup>TM</sup>) bulk powder carbon nanotubes were obtained from NanoIntegris, Inc. (Skokie, IL, USA), and SouthWest NanoTechnologies (Norman, OK, USA), respectively. Phage library lot #0141501 was purchased from New England Biolabs (Ipswich, MA, USA). Peptides used during characterization were ordered from Genescript, Inc. (Piscataway, NJ, USA).

### 2.1. Phage Display with CNT Target

Bulk powder HiPCO single-walled carbon nanotubes (NanoIntegris, Inc., Skokie, IL, USA) were washed with 70% ethanol and Tween-20 Tris-buffered saline (TBST) solution. Peptides were selected using the Ph.D.-12™ Phage Display Peptide Library (lot #0141501). Five total rounds of target binding, elution, and amplification were carried out according to the New England Biolabs' (NEB) instructions. The phage peptide library was incubated with washed HiPCO carbon nanotubes in TBST. Following several washes with (0.1–1.0% Tween-20) TBST, binding phage peptides were eluted using pH 2.2 glycine–HCl buffer and neutralized with pH 9.1 Tris–HCl buffer. Eluted binding phage underwent sequencing methods for each of the five rounds.

### 2.2. Phage Display Sans Target

Ph.D.-12 PD peptide phage library (lot #0141501) underwent five total rounds of amplification, according to the amplification portion of PD (NEB). The phage peptide library underwent the same treatment as the PD with CNT target samples, only without the CNT target. Amplified phages were sequenced by both methods for each of five rounds.

### 2.3. Sanger Sequencing

The phage eluate was plated onto individual X-gal/IPTG plates using *E. coli* ER2738 and grown at 37 °C in an Isotemp Incubator (Fisher Scientific (Waltham, MA, USA), CAT11-690-637D) overnight. Concentration of the phage sample was also calculated in plaque forming units for each round. Samples were then sent to Genewiz, Inc. (South Plainfield, NJ, USA) where they underwent Sanger sequencing.

### 2.4. High Throughput Sequencing

The sample phage eluate was run in a thermal cycler (GeneAmp PCR System 2400 (Perkin Elmer, Waltham, MA, USA) (94 °C, 2 min denature; 50 °C, 30 s anneal; 72 °C, 30 s extension; 25 × total). PCR products were isolated via gel purification (1.8% agarose gel, 200 V, Enduro Power Supplies, Labnet International, Inc., Edison, NJ, USA) and purified via DNA purification kits (QIAprep Spin Miniprep Kit, or QIAquick Gel Extraction Kit, Qiagen, Hilden, Germany). Samples were Illumina MiSeq 2 × 250 bp sequenced (Genewiz, Inc., South Plainfield, NJ, USA).

### 2.5. Dispersion Experiment

A carbon nanotube peptide solution (1 mg/mL bulk powder HiPCO carbon nanotubes, (1 mg/mL) peptide (Genescript, Inc., South Plainfield, NJ, USA), 3.5 mL total volume in water) was sonicated (VibraCell VC750 horn probe sonicator, Sonics, Newton, CT, USA) in pulse mode for 30 min (15 s on, 15 s off). Samples were centrifuged for 20 min (20,000 × *g*, Eppendorf 5810-R, Eppendorf, Enfield, CT, USA). The optical density of the supernatant was measured (350–1600 nm, 1 mL volume, 0.5 cm cuvettes, Cary 500 Scan UV–Vis–NIR Spectrophotometer, Agilent, Santa Clara, CA, USA).

### 2.6. Gold Decoration Experiment

#### 2.6.1. Characterization by Transmission Electron Microscopy (TEM)/Scanning Electron Microscopy (SEM)

Scanning Electron Microscopy (SEM) images were obtained on a FEI Quanta SEM microscope (FEI Company, Hillsboro, OR, USA) operating at 10 kV and at a working distance of 25 mm. Peptide dispersed CNT samples were deposited on electrodes and mounted on a standard SEM puck for imaging. Bright field Transmission Electron Microscopy (TEM) images were obtained on a Philips CM200 transmission electron microscope (Philips Research, Cambridge, MA, USA) operating at 200 kV or on an FEI CS-corrected Titan TEM microscope (FEI Company, Hillsboro, OR, USA) operating at 300 kV for high resolution TEM images. Samples were prepared by pipetting 10 µL of peptide dispersed carbon

nanotubes incubated with 20  $\mu\text{L}$  of 2 nm Au colloids (Ted Pella, Redding, CA, USA) onto 200 mesh copper TEM grid coated with an ultrathin carbon film and air dried.

### 2.6.2. Electrical Measurements by Dielectrophoresis (DEP)

A custom silicon wafer sensor chip (8.4 mm  $\times$  18 mm) with gold (Au) and titanium (Ti) metallization consisted of nine devices per chip (5  $\mu\text{m}$  gap for each electrode pair). CNTs were suspended in various peptide solutions (using the same parameters as in the dispersion method above) and drop casted (1  $\mu\text{L}$ ) onto each electrode gap on the sensor. Dielectrophoresis (DEP) was performed using conditions of 10 MHz frequency, 6 Vpp (peak to peak voltage), and 1 min exposure time set by the function generator (AFG1022 Function Generator, Tektronix, Beaverton, OR, USA), which was connected to the Signatone probe station (H100 Series Probe Station, Signatone, Gilroy, CA, USA). The probe station provided the contacts to the sensor. A 4200 semiconductor characterization system (Keithley, model # 4200-SCS, Solon, OH, USA) was connected to the probe station for data collection. Average resistance measurements after CNT–Peptide deposition are summarized in Table A3. After DEP, the sample was washed with distilled water and gently dried with an air flow. Colloidal AuNP were functionalized onto each device gap (over CNT–Peptides previously deposited) for 10 min. Current versus voltage measurements were taken after each step. The voltage was swept from  $-1$  V to 1 V in increments of 0.1 V during data collection.

## 3. Results and Discussion

### 3.1. Identification of Peptides

In this research, two commercial SWNTs were chosen for screening against the phage library. These included HiPCO<sup>TM</sup> (average diameter ( $\bar{d}_t$ ) = 1.05 nm and standard deviation ( $\sigma$ ) = 0.15 nm, a mixture of c.a. 50 different SWNTs, covering a range of chiralities [15–18]) and CoMoCAT<sup>®</sup> synthesized SG-65<sup>TM</sup> ( $\bar{d}_t$  = 0.81 nm  $\sigma$  = 0.15 nm, a mixture of c.a. 25 different SWNTs, primarily (6,5) chirality [19]). Figure 1 describes the PD workflow for both commercial SWNTs. Thirty phage clones of each round of amplification were analyzed by traditional Sanger DNA sequencing per the manufacturers' instructions (NEB, Inc., Ipswich, MA, USA) to yield an enriched sequence of TAKYLPMRPGPL (C1) (Table A1, Appendix A). This sequence dominated the population after three rounds of PD against both the CoMoCAT and HiPCO SWNTs. HTS (Illumina MiSeq, 2  $\times$  250 bp, NGS Genewiz, South Plainfield, NJ, USA) allowed for a much larger portion of the phage clone population to be sampled than the Sanger method, thus generating a “big picture” description, yielding over 14 million sequences. Due to the large number of sequences as well as the added amplification bias associated with HTS–PD, various analysis methods were investigated. Phage amplification at varying rates can be due to levels of infectivity, growth properties, binding to target or other contaminating materials, or possibly unsuccessful elution off of the target.

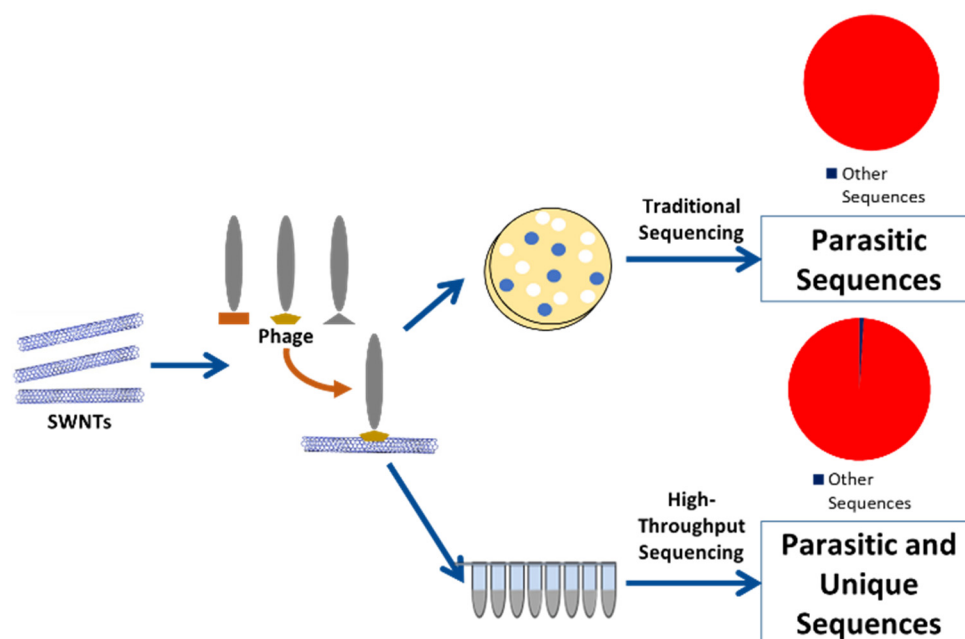


**Figure 1.** PD schematics showing the identification of binding peptides from both traditional and HTS–PD methods for SWNT target.

In traditional and in HTS–PD methods, phage peptide clones with high rates of amplification are frequently identified as the most abundant sequences and can be chosen as the binders to carbon nanotubes. In order to avoid sequences being falsely identified as high-affinity binders due to high amplification rates, amplification for each peptide sequence must be evaluated without the SWNT target present. These nonbinding high-proliferating (parasitic) sequences were identified through the full sample data for the naïve library (Ph.D-12, NEB), and the amplified library sans target. We performed the HTS–PD analysis for the naïve library to better understand the initial sequence frequencies and how they amplified in each round. Although an ideal library would contain  $\sim 10^{12}$  sequences in equal amounts, C1 was present in  $\sim 10\%$  of total sequences. As the library was amplified in the presence of the carbon nanotube target, C1 increased to greater than 94% in rounds three through five (Table A1). This particular peptide sequence tethered to the M13 phage outgrew and proliferated more rapidly than the other library members. It is also worth noting that this C1 sequence caused mutations through the increasing rounds of amplification. These mutant progeny were also prolific in the phage library population sans SWNTs (99%, rounds three and five) and with SWNTs (99%, rounds four and five). Using a traditional and/or HTS–PD method, this C1 sequence would be identified as a dominant high-affinity binder to SWNTs.

In order to remove these panning biases and uncover true high-affinity binders, a normalized-HTS PD method (NHTS–PD) was used to rank the peptide sequences by their preferential binding to each sample of carbon nanotube. First, the occurrences given in the high-throughput data sans target were normalized to the occurrences given in the high-throughput data with a carbon nanotube target for each data set and specific peptides were identified. Peptide sequences sans target increased in varying frequencies due to the differences in amplification rates from round to round of panning rather than from binding affinity. Each round of HTS data, with and without target, was analyzed by the fraction of occurrences in order to remove the influence of a variation among the total number of sequences for round to round consistency. Then, the fraction of occurrences sans target was subtracted out, peptide specific, from the fraction of occurrences with target, thus removing the amplification biases. If the fraction of occurrences of a specific peptide increased over multiple rounds after normalization, it was designated as a highly probable CNT binding

sequence. If the fraction of a specific peptide decreased after multiple rounds, the peptide amplified at a higher rate than binding and could be classified as parasitic. Peptides with near zero change indicated that they were not specific binders to the SWNTs. Finally, the curated datasets uncovered unique sequences that were enriched throughout multiple rounds of PD due to their binding to SWNTs (Table A1). The dominant occurrences of the parasitic sequence in the library complicated the enrichment of binding peptides as well as interpretation of the data in the traditional PD. In NHTS–PD, the normalization of the sequencing datasets of the phage library with and without target resulted in sequences enriched due to SWNT binding rather than due to phage proliferation rate biases.

The sequences from traditional PD were diverse in amino acid composition, revealing no observable trends in hydrophobicity and ionic property. However, the sequence compositions from NHTS–PD exhibited a consistency with previously reported studies showing a prevalence of aromatic amino acid residues (Tryptophan, Tyrosine, and Phenylalanine) that interact with CNTs, forming  $\pi$ - $\pi$  stacking [20,21]. The presence of Histidine and Tryptophan have been observed in CNT binding peptides (CBPs) [10,22,23] as well as Arginine to attract CNTs due to the formation of salt bridges [19,23]. No identical sequence to previous works was observed in our datasets. This could be due to (1) the difference in as-supplied PD library, (2) biases due to the sequence contamination and/or (3) the commercially available SWNT batches.

### 3.2. Peptide CNT Dispersion: Binding Characterization

We further exploited two of the top sequences from our unique NHTS–PD analysis (one with high affinity to HiPCO SWNTs, annotated as Peptide 8 (P8, LA–NAFAHRQRC), and one with high affinity to CoMoCAT SWNTs, annotated as Peptide 4 (P4, TPYVTHYSLNPF), to study their specific binding interactions. Binding properties of these peptides were then compared to the P1 (HSSYWYAFNNKT) sequence identified through previous research for all SWNTs through traditional Sanger methods and the C1 sequence identified as the parasitic nonspecific sequence through traditional Sanger and HTS–PD methods in this research. Binding characterization experiments were investigated against HiPCO CNTs due to the wide range of diameter distribution providing a better test sample towards the peptides' SWNT-diameter-based preference, when compared to the narrow diameter distribution of CoMoCAT samples.

The degree of dispersion indicates affinity to the CNTs. DNA [2,24], surfactants [25], and peptides [26] have all been investigated as CNT dispersants [26–28]. Surfactant like molecules with high affinity to CNTs were pursued to result in dense dispersion of CNTs. We hypothesized that the ability to disperse SWNTs in aqueous media was related to the affinity of the peptide to the nanotube surface. The extreme surface area and cohesive energy between adjacent SWNTs naturally drives the tubes to form strong aggregates in commercially obtained nanotubes thus causing difficulty in aqueous dispersion [29]. SWNTs are incompatible with polar aprotic solvents which make the downstream processing of the tubes much more challenging than other conventional materials [9,30]. Achieving a uniform dispersion of individual tubes in solution has been a prerequisite process to build high performance single-tube level electronic devices [5,20].

Since all the peptides were readily soluble in aqueous media at a 1 mg/mL concentration, the effect of peptide solubility on SWNT dispersion was assumed to be negligible. The observed optical absorption spectra of SWNT dispersions were analyzed with various dispersants including NHTS–PD identified HiPCO binding peptide, P8 (1 mg/mL, Table A2), NHTS–PD identified CoMoCAT binding peptide, P4 (1 mg/mL, Table A2) and literature identified HTS–PD peptide, P1 (1 mg/mL, Table A2) [31].

As previously shown, the supernatants containing P1 displayed high ability to disperse the CNTs [24,32]. As shown in Figure 2, the absorbance spectra was compared for peptides identified using the traditional method versus the NHTS–PD method and compared to the previous peptide found in literature (P1) [10]. Figure 2A shows the differences in dispersion by P8 (identified using NHTS–PD methods to HiPCO), P4 (identified using

NHTS–PD methods to CoMoCAT), C1 (parasitic sequence identified using traditional methods), and P1 [14] in terms of the extent of dispersed HiPCO CNTs. It was noticeable that the absorbance profiles,  $E_{11}^S$ , denoting the transition between the valence and conduction bands of the semiconducting SWNT, varied between P1, P4, and P8. Since the  $E_{11}^S$  was inversely related to the SWNT diameter, it was hypothesized that peptides can recognize CNTs possessing varying properties. Moreover, CoMoCAT represented smaller diameter SWNTs than HiPCO and could impose more challenges in PD due to an increase in tube circumferential curvature and cohesive energy. However, the HTS-assisted PD peptides showed a striking affinity to the small diameter SWNT sample by showing a pitch-black aqueous nanotube dispersion in P4. C1, as expected as the contaminant sequence, was not a strong specific CNT binder shown by near baseline absorption and clear colorless dispersion (Figure 2B), likely a product of traditional PD bias.

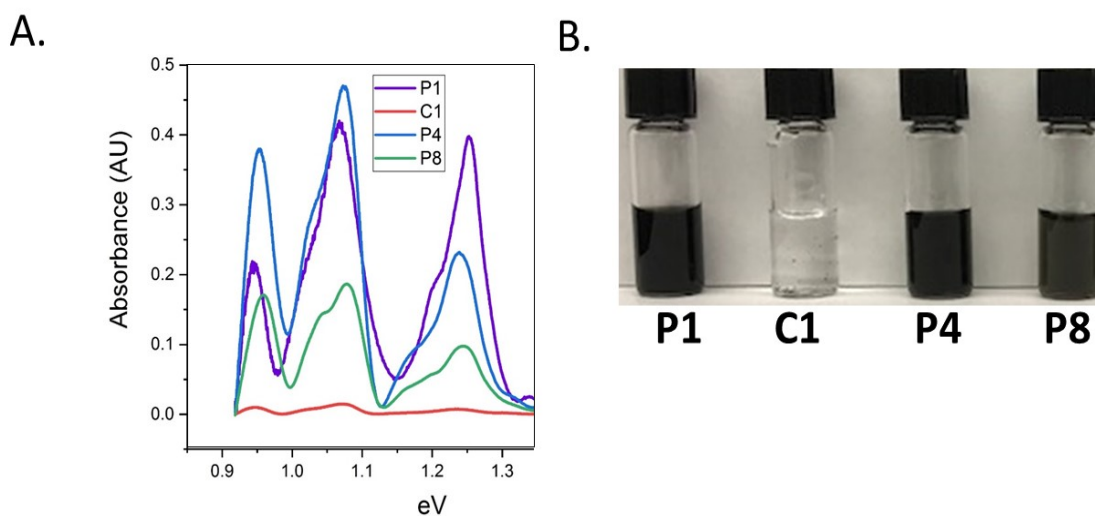


**Figure 2.** (A) Absorption spectra of CNT–peptide dispersed solutions and (B) optical micrograph of aqueous dispersion of HiPCO CNT dispersion obtained from the peptides identified by literature (P1 peptide), non-HTS method (C1) and NHTS–PD method (peptide P4 and P8).

The  $E_{11}^S$  NIR Spectra can be deconvoluted and analyzed to better understand the chirality/diameter properties of the semiconducting HiPCO CNT dispersion. Theoretically, each deconvoluted peak corresponds to several different chirality CNTs and thus can be used to determine the concentration of a group of chirality tubes dispersed by each peptide [4,33–36]. Since the overlap between metallic and semiconducting electronic transition energy impedes the use of full UV–NIR profiles to obtain the chirality/diameter specific analysis of these CNT samples, we strictly used the  $E_{11}^S$  absorbance of 0.925–1.45 eV to retrieve the SWNT diameter profiles from the dispersions [24,33].

Each peak wavelength corresponded to multiple chirality CNTs of similar diameter. The lower the wavelength, the higher the optical transition energy, and thus the smaller the diameter of corresponding SWNT. Because of this, a trend can be observed for the dispersion of CNTs based on their diameters. Figure 3A shows the deconvolution of the  $S_{11}$  semiconducting range from HTS identified CoMoCAT binding peptide (peptide 4), and Figure 3B from HTS identified HiPCO binding peptide (P8) thus suggesting chirality-specific binding. P8 showed dispersion of CNTs in the diameter range commonly seen for HiPCO CNTs ( $1.05 \pm 0.15$  nm [36]). P4 showed dispersion mainly of CNTs with a diameter commonly corresponding to (6,5) CNTs ( $0.81 \pm 0.08$  nm [19]).

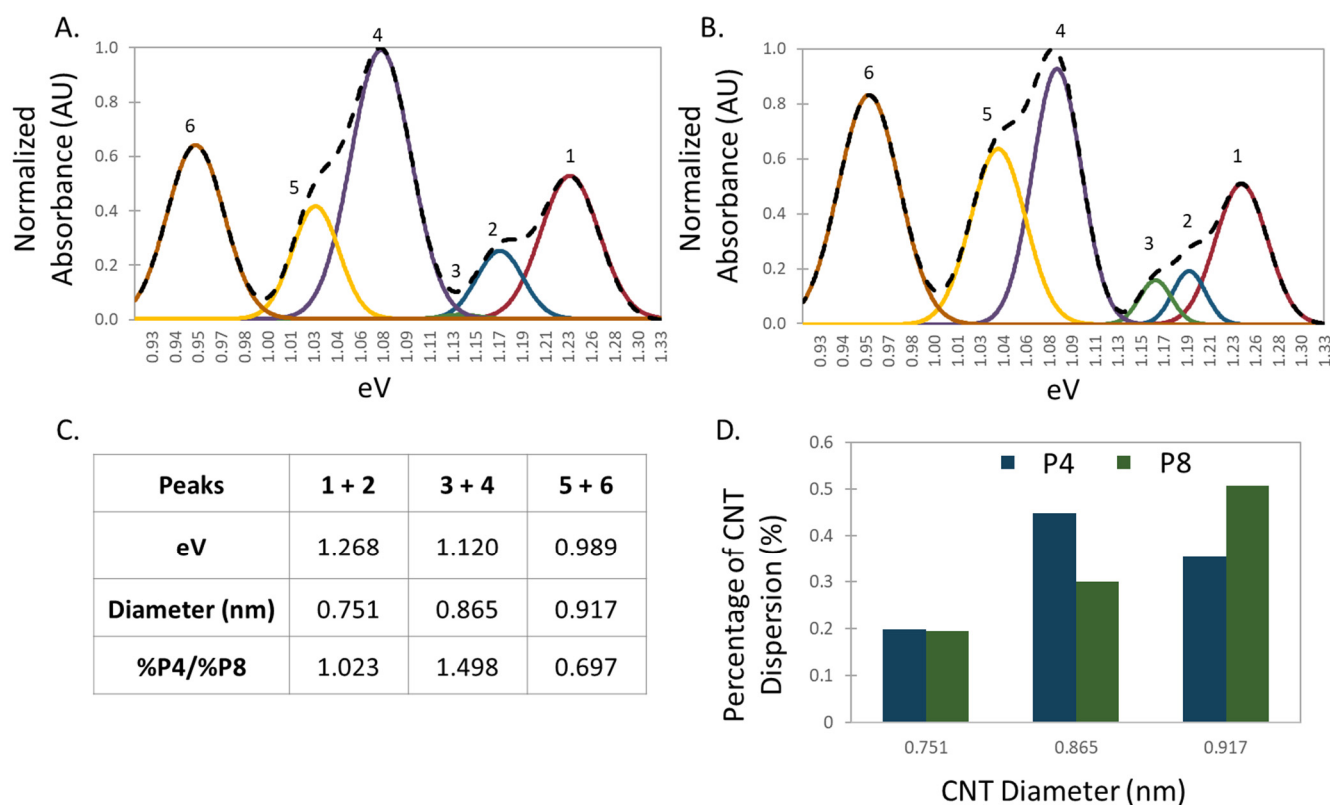


**Figure 3.** Deconvoluted spectra of (A) CoMoCAT dispersion with binding peptide, P4, and (B) HiPCO dispersion with P8 peptide, dispersing HiPCO CNTs. All absorbance data are presented in the semiconducting S11 range. (C) Peaks were separated by small (0.751 nm), medium (0.865 nm), and large (0.917 nm) SWNT diameter to (D) compare diameter dependent dispersion for CoMoCAT and HiPCO identified binding peptides.

It can be seen in Figure 3C,D that P4 had a higher affinity for smaller diameter CNTs, while P8 had a higher affinity for larger diameters. This trend of dispersion based on diameter can be better understood by dividing the spectra in Figure 3A,B into arbitrary “zones” for analysis based on small, medium, and large diameters. The CNTs dispersed in each of the diameter ranges (small: peaks 1 and 2, medium: peaks 3 and 4, and large: peaks 5 and 6, annotated in Figure 3C) can be compared as a proportion of absorbance (P4:P8, or %P4/%P8), which is referred to as the dispersion ratio of CoMoCAT (P4) to HiPCO (P8). These values can be analyzed and compared to their corresponding average diameter CNTs (Figure 3C,D). This analysis supported the claim that that P8 has a higher affinity for large diameter CNTs while P4 has a higher affinity for small/medium diameter CNTs. It was expected for P8 to have a high dispersion value for medium diameter tubes in the range of HiPCO diameter tubes (average 0.94 nm) as it was selected to HiPCO tubes. P4, selected for the smaller diameter CoMoCAT tubes, was seen to disperse tubes of small/medium diameters (average 0.78 nm). These results support the selectivity of peptides to CNTs of differing diameters and chirality as well as the success of this high-throughput analysis method to identify diameter specific peptides.

### 3.3. SWNT Functionalized with Gold Nanoparticles (AuNP) Using Multifunctional Peptides

A benefit of identifying CBPs is the ability to hybridize CNTs with varying molecules, sensing elements, or optically active nanoparticles for potential application to biosensors, catalysis, biomedicine, etc. Using the known gold-binding peptide, A3, (AYSSGAPMPPF) [31], CNTs can be decorated with gold nanoparticles (AuNP) by creating a fusion peptide containing both A3 and CNT-binding sequences. For example, a P4A3 fusion peptide was used to coat HiPCO CNTs and direct the precise assembly of 2 nm AuNPs on the peptide coated CNT surface. Assembly of gold with peptide–CNT revealed differing degrees of

organization of AuNPs on the CNT surface depending on peptide sequence and presence of gold-binding peptide. Both P4 and P4A3 notably assembled the AuNPs, however, the P4A3 peptide appeared to allow for a higher density of AuNP assembly than the P4 peptide (Figure 4A). These AuNPs were uniformly spaced along the CNT surface and showed an interparticle spacing of  $1.68 \pm 0.74$  nm (P4) and  $1.35 \pm 0.68$  nm (P4A3) by high resolution TEM.

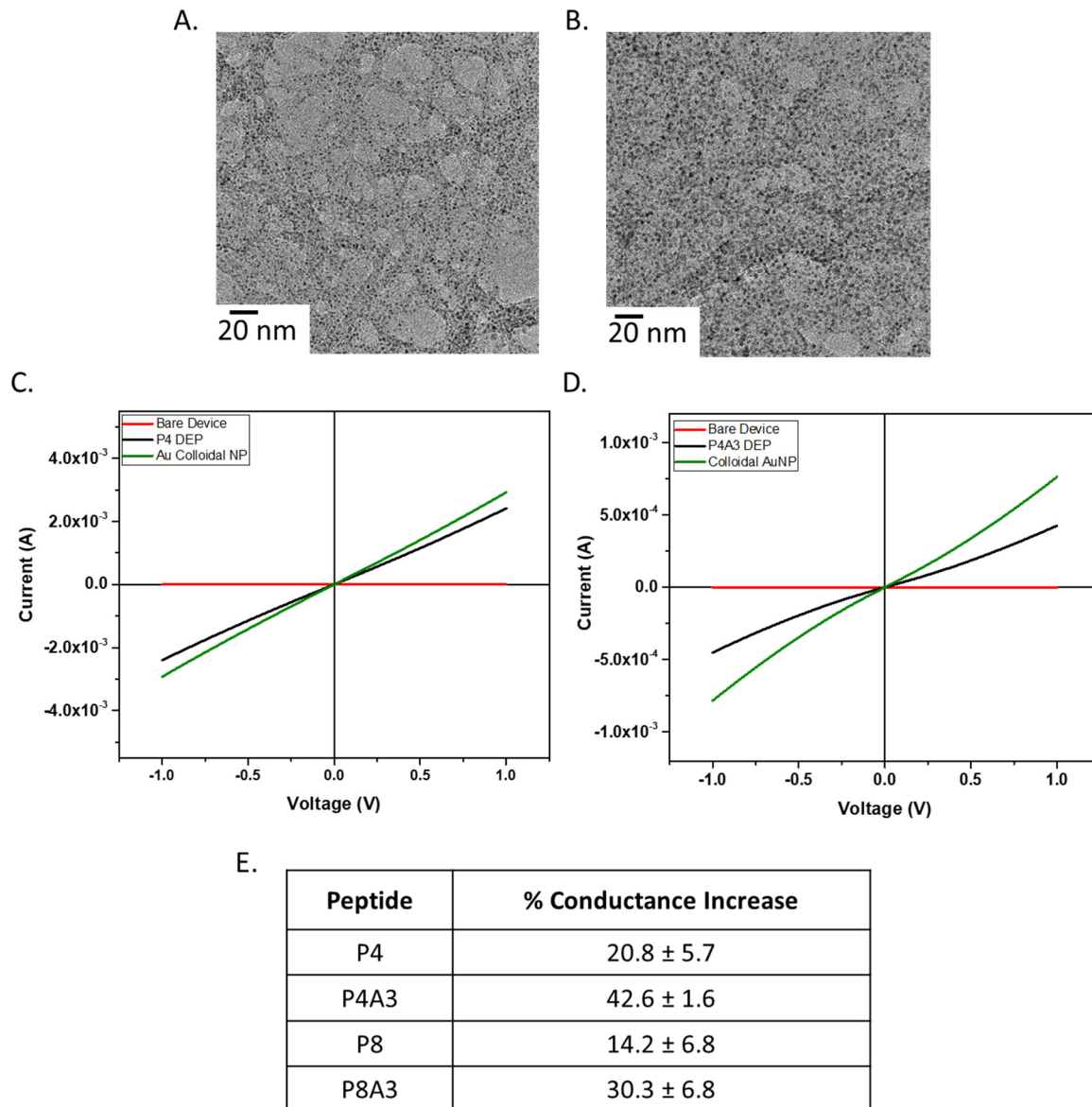


**Figure 4.** (A,B) HiPCO CNTs dispersed by peptide solutions were used to decorate 2 nm AuNPs with HiPCO CNTs (TEM) ((A): P4, (B): P4-A3). (C,D) IV measurements from bare surface (red), peptide ((C): P4, (D): P4A3) + CNT (black) and peptide + CNT + colloidal AuNPs (green). (E) Conductance increased after addition of AuNP confirming successful AuNP decoration on CNT by fusion peptides.

In order to better understand how the binding behavior of the peptides with AuNP affect electrical properties of CNT assembly, voltage versus current measurements were taken. Custom silicon based sensors consisted of electrode pairs which underwent a dielectrophoresis (DEP) process to deposit the peptide functionalized CNTs. DEP utilized alternating current (AC electrical field) to produce dielectrophoretic forces that propagated and assembled CNT onto areas of interest. Depositing CNT onto specific locations enabled

the bridging of the electrode pairs which produced a conductive channel. This method allowed the precise control of CNT deposition with designated electrodes. The current versus voltage (IV) plots showed noticeable changes pre/post exposure to colloidal AuNP (Figure 4B). The overall increase in conductance post AuNP assembly could be related to the lowered electron tube-to-tube tunnelling barrier, corresponding to the TEM observation on selective AuNP decoration to CNTs. Moreover, the designer fusion peptides, P4A3 and P8A3, showed noticeable  $42.6 \pm 1.6\%$  and  $30.3 \pm 6.8\%$  conductance increase for the DEP assembled SWNT, respectively (Figure 4C). Meanwhile, the native SWNT binding peptides, P4 and P8 only, showed a lower percent increase in the DEP SWNT conductance ( $20.8 \pm 5.7\%$  and  $14.2 \pm 6.8\%$ , respectively) as compared to the fusion peptides. This was as expected due to the tighter interparticle spacing for the A3-terminated CBPs as compared to the native CBPs. Overall, observations made from the TEM and conductance measurement to the DEP assembled CNT samples indicated that the multifunctional peptides allowed for a successful nanoscale property control of the native CNTs, as designed.

#### 4. Conclusions

Inherent biases of amino acid prevalence within the native library as well as varying rates of amplification among the different phage clones within the library complicate traditional PD selection and must be overcome in order to generate successful results. In order to uncover the useful data in the binding sequences, a method must be discovered to remove the biases from the analysis.

Traditional and HTS-PD methods were investigated and compared to a newly identified NHTS-PD method. This NHTS-PD method successfully identified and removed parasitic sequences, which amplified at very high rates yet were not binding, and thus were clouding the sequencing data. Using only traditional and HTS-PD methods, these parasitic sequences would have been identified as high-affinity SWNT binders. A highly mutating sequence, C1, was discovered as a library contaminant and possibly a tag or mutation in the phage sequence. The NHTS-PD method was able to identify this and many other peptides as false positive binding sequences and uncover sequences specific for classes of carbon nanotubes solely due to the binding properties.

From the obtained results, it can be concluded that peptides identified by the unique NHTS-PD analysis method can specifically select for CNTs with different properties. This analysis method can be used for all other high throughput sequencing based selection methods to uncover unique binding recognition elements, and prevent false binding sequences from clouding true high affinity binders. In this research, a new peptide selective for HiPCO CNTs and a new peptide selective for CoMoCAT CNTs were identified. These two peptides vary in selectivity as P8, selected for HiPCO CNTs, has a higher affinity for large diameter CNTs (in the range of HiPCO diameters), while P4, selected for CoMoCAT, has a higher affinity for small diameter CNTs (in the range of CoMoCAT diameter) than traditionally identified CNT binding peptides. Using the NHTS-PD analysis method developed in this research can uncover unique peptides selective for specific diameter and possibly even single chirality CNTs. This method is capable of identifying and removing nonbinding parasitic sequences not only for CNTs but for other targets of interest, thus increasing the probability of selecting a high-affinity binding peptide.

**Author Contributions:** Conceptualization, R.K., C.H., S.K. and R.N.; methodology, R.K. and C.H.; software, R.K.; validation, R.K., J.S. and Y.N.; formal analysis, R.K. and S.K.; investigation, R.K.; data curation, R.K.; writing—original draft preparation, R.K.; writing—review and editing, R.K., S.K. and R.N.; visualization, R.K.; supervision, R.N.; project administration, R.N.; funding acquisition, R.N. All authors have read and agreed to the published version of the manuscript.

**Funding:** This work was supported by the Air Force Office of Scientific Research and the Air Force Research Laboratory.

**Acknowledgments:** This research was performed while R.K. held a Dayton Area Graduate Studies Institute graduate student fellowship. We acknowledge support from the Air Force Office of Scientific Research.

**Conflicts of Interest:** The authors declare no conflict of interest.

## Appendix A

**Table A1.** Sequencing results for round 5 of traditional Sanger and traditional high throughput methods compared to round 5 of NHTS-PD <sup>1</sup>.

Traditional Method:				Unique Method:	
Sanger		HTS		NHTS-PD	
CoMoCAT	HiPCO	CoMoCAT	HiPCO	CoMoCAT	HiPCO
TAKYLMRPGPL	TAKYLMRPGPL	TAKYLMRPGPL	TAKYLMRPGPL	AVYQSKVLAR	GSVQKLSATPWV
QASDSLRSVGP	QASDSLRSVGP	AVYQSKVLAR	TANYLMRPGPL	GSVQKLSATPWV	GLRETQVTALQK
TAKYLMRPGPL	TFNTEAMWTSW*	GSVQKLSATPWV	TAKYLPLRPGPL	SVDGWLEPPTST	LADNAFAHRQRC
SAKYLMRPGPL*	WEGGGAGKLSAA*	SVDGWLEPPTST	TAQYLMRPGPL	ALNWTELHGQAT	MGNVSHQPIPLP
DVAKSYQSFNE*	AVYQSKVLAR*	TANYLMRPGPL	TAKYLMRPGPL	DAATQGVLARHY	SHVDQMHRPHRP
HLEALSDLVNRN*	FNDGSSKPLDDL*	ALNWTELHGQAT	TAKYLMRPGPL	TPYVTHYSLNPF	YGHLEPPTPREL
DAATQGVLARHY*	ALNWTELHGQAT*	DAATQGVLARHY	TAKYLMRPGPL	NSYASPLEPKVS	VPDRLVAYPIVL
GLGPALHHNIVA*	SPHSAASVLASL*	TAKYLPLRPGPL	TARYLMRPGPL	FNDGSSKPLDDL	IANPSLFPMSM

<sup>1</sup> Sequences occurring only once in results are designated by an asterisk (\*).

**Table A2.** Identified peptide sequences used in binding characterization experiments.

ID	Peptide Sequence	Identified
P1	HSSYWYAFNNKT	HTS-PD Literature to CNT
C1	TAKYLMRPGPL	Traditional to CNT
P4	TPYVTHYSLNPF	NHTS-PD to CoMoCAT
P8	LADNAFAHRQRC	NHTS-PD to HiPCO

**Table A3.** Average resistance measurements after CNT-Peptide deposition.

Peptide	Average Resistance (Ohms)
P4	342 ± 36.1 Ω
P4A3	2065 ± 367.8 Ω
P8	560 ± 200.1 Ω
P8A3	1128 ± 292.5 Ω

## References

- Zheng, M.; Semke, E.D. Enrichment of Single Chirality Carbon Nanotubes. *Amer. Chem. Soc.* **2007**, *129*, 6084–6085. [[CrossRef](#)]
- Zheng, M.; Jagota, A.; Semke, E.D.; Diner, B.A.; McLean, R.S.; Lustig, S.R.; Richardson, R.E.; Tassi, N.G. DNA-Assisted Dispersion and Separation of Carbon Nanotubes. *Nat. Mater.* **2003**, *2*, 338–342. [[CrossRef](#)]
- Tromp, R.M.; Afzali, A.; Freitag, M.; Mitzi, D.B.; Chen, Z. Novel Strategy for Diameter-Selective Separation and Functionalization of Single-Wall Carbon Nanotubes. *Nano Lett.* **2008**, *8*, 469–472. [[CrossRef](#)] [[PubMed](#)]
- O’Connell, M.J.; Bachilo, S.M.; Huffman, C.B.; Moore, V.C.; Strano, M.S.; Haroz, E.H.; Rialon, K.L.; Boul, P.J.; Noon, W.H.; Kittrell, C.; et al. Band Gap Fluorescence From Individual Single-Walled Carbon Nanotubes. *Science* **2002**, *297*, 593–596. [[CrossRef](#)]
- Kuang, Z.; Kim, S.N.; Goodson, W.; Farmer, B.L.; Naik, R.R. Biomimetic Chemosensor: Designing Peptide Recognition Elements for Surface Functionalization of Carbon Nanotube Field Effect Transistors. *ACS Nano* **2010**, *4*, 452–458. [[CrossRef](#)] [[PubMed](#)]
- Politi, J.; Zappavigna, S.; Rea, I.; Grieco, P.; Calì, A.; Luce, A.; Caraglia, M.; De Stefano, L. Peptide Functionalization of Silicon for Detection and Classification of Prostatic Cells. *J. Sens.* **2017**, *2017*, 6792396. [[CrossRef](#)]
- Ermini, M.L.; Song, X.C.; Špringer, T.; Homola, J. Peptide Functionalization of Gold Nanoparticles for the Detection of Carcinoembryonic Antigen in Blood Plasma via SPR-Based Biosensor. *Front. Chem.* **2019**, *7*, 40. [[CrossRef](#)]

8. Sim, D.; Krabacher, R.; Chávez, J.L.; Martin, J.A.; Islam, A.E.; Kuang, Z.; Maruyama, B.; Naik, R.R.; Kim, S.S. Peptide-Functionalized Single-Walled Carbon Nanotube Field-Effect Transistors for Monitoring Volatile Organic Compounds in Breath. In Proceedings of the IEEE International Flexible Electronics Technology Conference, Vancouver, BC, Canada, 11–14 August 2019.
9. Sapsford, K.E.; Algar, W.R.; Berti, L.; Gemmill, K.B.; Casey, B.J.; Oh, E.; Stewart, M.H.; Medintz, I.L. Functionalizing Nanoparticles with Biological Molecules: Developing Chemistries that Facilitate Nanotechnology. *Chem. Rev.* **2013**, *113*, 1904–2074. [[CrossRef](#)]
10. Pender, M.J.; Sowards, L.A.; Hartgerink, J.D.; Stone, M.O.; Naik, R.R. Peptide-Mediated Formation of Single-Wall Carbon Nanotube Composites. *Nano Lett.* **2006**, *6*, 40–44. [[CrossRef](#)]
11. Cui, Y.; Kim, S.N.; Naik, R.R.; McAlpine, M.C. Biomimetic Peptide Nanosensors. *Acc. Chem. Res.* **2011**, *45*, 696–704. [[CrossRef](#)]
12. Naik, R.R.; Jones, S.E.; Murray, C.J.; McAuliffe, J.C.; Vaia, R.A.; Stone, M.O. Peptide Templates for Nanoparticle Synthesis Derived from Polymerase Chain Reaction-Driven Phage Display. *Adv. Funct. Mater.* **2004**, *14*, 25. [[CrossRef](#)]
13. Van Dorst, B.; Mehta, J.; Rouah-Martin, E.; Blust, R.; Robbens, J. Phage Display as a Method for Discovering Cellular Targets of Small Molecules. *Methods* **2012**, *58*, 56–61. [[CrossRef](#)]
14. Qianglong, Z.; Shi, L.; Peng, G.; Fei-Shi, L. High-throughput sequencing technology and its application. *J. Northeast. Agric. Univ.* **2014**, *21*, 84–96.
15. Kukovec, A.; Kramberger, C.; Georgakilas, V.; Prato, M.; Kuzmany, H. A detailed Raman study on thin single-wall carbon nanotubes prepared by the HiPCO process. *Eur. Phys. J. B-Condens. Matter Complex Syst.* **2002**, *28*, 223–230. [[CrossRef](#)]
16. Bachilo, S.M.; Balzano, L.; Herrera, J.E.; Pompeo, F.; Resasco, D.E.; Weisman, R.B. Narrow (n,m)-Distribution of Single-Walled Carbon Nanotubes Grown Using a Solid Supported Catalyst. *J. Am. Chem. Soc.* **2003**, *125*, 11186–11187. [[CrossRef](#)]
17. Chen, Y.; Ciuparu, D.; Lim, S.; Yang, Y.; Haller, G.L.; Pfefferle, L. Synthesis of Uniform Diameter Single-Wall Carbon Nanotubes in Co-MCM-41: Effects of the Catalyst Prereduction and Nanotube Growth Temperatures. *J. Catal.* **2004**, *225*, 453–465. [[CrossRef](#)]
18. Luo, Z.; Pfefferle, L.D.; Haller, G.L.; Papadimitrakopoulos, F. (n, m) Abundance Evaluation of Single-Walled Carbon Nanotubes by Fluorescence and Absorption Spectroscopy. *J. Am. Chem. Soc.* **2006**, *128*, 15511–15516. [[CrossRef](#)]
19. Kitiyanan, B.; Alvarez, W.; Harwell, J.; Resasco, D. Controlled production of single-wall carbon nanotubes by catalytic decomposition of CO on bimetallic Co-Mo catalysts. *Chem. Phys. Lett.* **2000**, *317*, 497–503. [[CrossRef](#)]
20. He, Z.; Zhou, J. Probing Carbon Nanotube-Amino Acid Interactions in Aqueous Solution with Molecular Dynamics Simulations. *Carbon* **2014**, *78*, 500–509. [[CrossRef](#)]
21. LeMieux, M.C.; Roberts, M.; Barman, S.; Jin, Y.W.; Kim, J.M.; Bao, Z. Self-Sorted, Aligned Nanotube Networks for Thin-Film Transistors. *Science* **2008**, *321*, 101–104. [[CrossRef](#)]
22. Brown, S.; Jespersen, T.; Nygård, J. A Genetic Analysis of Carbon-Nanotube-Binding Proteins. *Small* **2008**, *4*, 416–420. [[CrossRef](#)]
23. Su, Z.; Leung, T.; Honek, J.F. Conformational Selectivity of Peptides for Single-Walled Carbon Nano-tubes. *J. Phys. Chem. B* **2006**, *110*, 23623–23627. [[CrossRef](#)]
24. Kim, S.N.; Singh, K.M.; Ouchen, F.; Grote, J.G.; Naik, R.R. DNA Mediated Solubilization of Single Wall Carbon Nano-tubes. In Proceedings of the 2008 IEEE National Aerospace and Electronics Conference, Dayton, OH, USA, 16–18 July 2008; pp. 94–96.
25. Rastogi, R.; Kaushal, R.; Tripathi, S.K.; Sharma, A.L.; Kaur, I.; Bharadwaj, L.M. Comparative Study of Carbon Nanotube Dispersion Using Surfactants. *J. Colloid Interface Sci.* **2008**, *328*, 421–428. [[CrossRef](#)]
26. Li, Z.; Kameda, T.; Isoshima, T.; Kobatake, E.; Tanaka, T.; Ito, Y.; Kawamoto, M. Solubilization of Single-Walled Carbon Nanotubes Using a Peptide Aptamer in Water below the Critical Micelle Concentration. *Langmuir* **2015**, *31*, 3482–3488. [[CrossRef](#)] [[PubMed](#)]
27. Pantarotto, D.; Partidos, C.D.; Hoebeke, J.; Brown, F.; Kramer, E.; Briand, J.-P.; Muller, S.; Prato, M.; Bianco, A. Immunization with Peptide-Functionalized Carbon Nanotubes Enhances Virus-Specific Neutralizing Antibody Responses. *Chem. Biol.* **2003**, *10*, 961–966. [[CrossRef](#)] [[PubMed](#)]
28. Pinals, R.L.; Ledesma, F.; Yang, D.; Navarro, N.; Jeong, S.; Pak, J.E.; Kuo, L.; Chuang, Y.-C.; Cheng, Y.-W.; Sun, H.-Y.; et al. Rapid SARS-CoV-2 spike protein detection by carbon nanotube-based near-infrared nanosensors. *Nano Lett.* **2021**, *21*, 2272–2280. [[CrossRef](#)] [[PubMed](#)]
29. Tohidifar, L.; Hadipour, N.L. Tracing chirality, diameter dependence, and temperature-controlling of single-walled carbon nanotube non-covalent functionalization by biologically compatible peptide: Insights from molecular dynamics simulations. *J. Mol. Modeling* **2019**, *25*, 274. [[CrossRef](#)]
30. Chiu, C.-C.; Dieckmann, G.R.; Nielsen, S.O. Role of Peptide-Peptide Interactions in Stabilizing Peptide-Wrapped Single-Walled Carbon Nanotubes: A Molecular Dynamics Study. *Pept. Sci. Orig. Res. Biomol.* **2009**, *92*, 156–163. [[CrossRef](#)]
31. Kim, S.N.; Kuang, Z.; Slocik, J.M.; Jones, S.E.; Cui, Y.; Farmer, B.L.; McAlpine, M.C.; Naik, R.R. Preferential Binding of Peptides to Graphene Edges and Planes. *J. Am. Chem. Soc.* **2011**, *133*, 14480–14483. [[CrossRef](#)] [[PubMed](#)]
32. Duan, W.H.; Wang, Q.; Collins, F. Dispersion of Carbon Nanotubes with SDS Surfactants: A Study From a Binding Energy Perspective. *Chem. Sci.* **2011**, *2*, 1407–1413. [[CrossRef](#)]
33. Kim, S.N.; Singh, K.; Ouchen, F.; Grote, J.G.; Naik, R.R. Solubilization of Single Wall Carbon Nanotubes with Salmon Sperm DNA. *TechConnect Briefs.* **2008**, *1*, 132–135.
34. Miyata, Y.; Yanagi, K.; Maniwa, Y.; Kataura, H. Optical Evaluation of the Metal-to-Semiconductor Ratio of Single-Wall Carbon Nanotubes. *J. Phys. Chem.* **2008**, *112*, 13187–13191. [[CrossRef](#)]

- 
35. Gravely, M.; Safae, M.M.; Roxbury, D. Oligonucleotide Length Determines Intracellular Stability of DNA-Wrapped Carbon Nanotubes. *bioRxiv* **2019**, 642413. [[CrossRef](#)]
  36. Oyama, Y.; Saito, R.; Sato, K.; Jiang, J.; Samsonidze, G.; Grüneis, A.; Miyauchi, Y.; Maruyama, S.; Jorio, A.; Dresselhaus, G.; et al. Photoluminescence Intensity of Single Wall Carbon Nanotubes. *Carbon* **2006**, *44*, 873–879. [[CrossRef](#)]